X-651-71-116
PREPRINT

NASA TM X-65551

OBSERVATIONS OF THE SOLAR LONG TERM VARIABILITY AND IRRADIANCE IN THE NEAR AND FAR ULTRAVIOLET

DONALD F. HEATH

FEBRUARY 1971

GSFC
GODDARD SPACE FLIGHT CENTER
GREENBELT, MARYLAND

X-651-71-116

OBSERVATIONS OF THE SOLAR LONG TERM VARIABILITY AND IRkADIANCE IN THE NEAR AND FAR ULTRAVIOLET

Donald F. Heath

February 1971

Goddard Space Flight Center

Greenbelt, Maryland 20771

ABSTRACT

Satellite observations of the ultraviolet solar flux at selected wavelength bands between 1200 and 3000A have been made continuously by a broad band photometer on Nimbus 3 (launched April 1969) and Nimbus 4 (launched April 1970). In addition, measurements have been made at 12 wavelengths from 2550-3400A which views the sun once per orbit from Nimbus 4. Two UV active regions with a 27 day period have been observed since the launch of Nimbus 3. UV flux variations decrease rapidly with wavelengths measuring from 1200A to 3000A. Twenty-seven day variations in the Lyman-α and 1350-1600A channel has declined from a maximum variability of 40% (solar rotation No. 1548) to about 7% after 20 solar rotations. At 1800Å the 27 day variability has declined from 6% to 4% over the same period. The UV activity observed at these wavelengths correlates with both the variations in the 10.7 cm flux and with the daily ΣK_p index (when > 40) as well as with certain observed UV active regions. The maxima in ΣK_p occur generally 1-3 days after the UV maxima. Considering similar measurements from a rocket flight in 1966 together with the Nimbus 3 and 4 observations, it is evident that there is also a very significant variation of the solar UV flux at 1800Å, which originates in regions of low solar temperatures, with the 11 year solar cycle.

An experiment designated MUSE (Monitor of Ultraviolet Solar Energy) was designed to measure the absolute solar flux in the 1100-3000A region over wavelength intervals of several hundred Angstroms and its possible vatiations over long time intervals. Solar energy in this region represents the major radiative energy input into the lower thermosphere, mesosphere, and upper stratosphere. This wavelength range also covers the transition from photospheric to chromospheric radiation which passes through the region of the solar temperature minimum.

The measurements reported here are from a test flight of the satellite instrument which was flown to an altitude of 210 km on an Aerobee 150 rocket (inertially stabilized to point at the sun) from the White Sands Missile Range on August 29, 1966, and subsequent flights on the Nimbus 3 and 4 satellites. The satellites were launched on April 14, 1969 and April 8, 1970 respectively. Both satellite instruments are still operating. The orbits of Nimbus 3 and 4 are sun synchronous, polar, and at a nominal altitude of 1100 km where the ascending node crosses the equator at approximately noon.

The same group of three sensors has been flown on the rocket, and the Nimbus 3 and 4 satellites. A comparison of the observations from the rocket flight with the initial results from the satellites has provided an indication of the 11 year solar cycle variations of the uv solar flux. The rocket flight in 1966 was during a period of low solar activity, while the 1969 launch of Nimbus 3 took place slightly past peak of the solar maximum. The launch of Nimbus 4

one year later has provided additional evidence for the solar cycle variability of the uv flux.

The correctness of the broad band photometric measurements of MUSE has verified by the observations with a double monochromator also on Nimbus 4 which measures in addition to the earth radiance, the solar irradiance within a 10A bandpass at 12 discrete wavelengths from 2550 to 3400Å once per orbit.

INSTRUMENT

The MUSE experiment consists of five vacuum photodiodes which were fabricated by the EMR Photoelectric Division of Weston Instruments, Inc. The photodiodes have a nominal 90° field of view, and they are mounted between bays of the Nimbus sensory ring in the direction of 180° from the velocity vector of the spacecraft. The sensors are fully illuminated by the sun for about 20 min of each 107 min orbit, and they view the sun at near normal incidence when crossing the terminator in the north polar regions. The angle of solar illumination to the normal of the face of the sensors is provided by an Adcole Corp. solar aspect sensor.

The short wavelength response is determined by a suitable radiation resistant optical filter [Heath and Sacher, 1966]. The long wavelength cutoff is achieved through the use of photocathode materials of varying degrees of "solar blindness." The response functions for the three photometer channels reported in this work are shown in figure 1. Sensor A consists of a MgF_2 window in front

of an opaque tungsten photocathode. Sensor B consists of an outer Al_2O_3 element backed by a fused SiO_2 filter, and a semi-transparent CuI photocathode which is deposited on an Al_2O_3 window. The third sensor, C, consists of an outer Al_2O_3 element and backed by a neutral density filter, and elements of fused SiO_2 and $CaCO_3$ (calcite). The CsTe semitransparent photocathode is deposited on an Al_2O_3 window. The outer Al_2O_3 elements of B and C have a vacuum deposited metallic grid for electrical shielding.

The photodiode currents are amplified by an automatic four decade range-switching amplifier. The dynamic range is from 10^{-12} amperes, the minimum discernable current on the most sensitive range to 10^{-7} amperes full-scale on the least sensitive range. The linear electrometer is automatically zeroed on every 48 sec program cycle. An in-flight calibration of the electrometer is made by sequentially sampling constant current sources every 48 sec. The constant current sources, are unaffected by temperature on the space environment, ionization chambers which are excited by Americium 210 foils. The typical dark current of the photodiodes is nominally 10^{-14} amperes.

The current outputs from the photodiodes are sequentially switched by reed relays into a common electrometer for 5 sec of each 48 sec cycle. The electrometer output was sampled at 1 sec intervals on Nimbus 3, and at 0.5 sec intervals on Nimbus 4.

At the Nimbus altitude a small portion of the sunlit earth subtends a solid angle of ~ 0.15 steradian. The contribution to solar signal at the terminator is

about a part in 10^{-3}, 10^{-4}, and 10^{-2} respectively for sensors A, B, and C respectively.

RADIOMETRIC CALIBRATION

The basis for directly comparing the uv solar flux measured from the rocket in 1966 and that from the Nimbus Satellites 3 and 4 in 1969 and 1970 respectively has been a standard vacuum photodiode which consists of a semi-transparent CsTe photocathode deposited on a Al_2O_3 window. Initially in 1966 the diode was calibrated at 2537Å against a Eppley Thermopile which had been calibrated against a standard of total irradiance. The calibration of the diode at 2537Å was used to calibrate a freshly deposited film of sodium salicylate in front of a photomultiplier which also was calibrated at 1216Å with a calibrated NO cell. Assuming the response of the sodium salicylate film to be constant over this wavelength range, the two end point calibrations agreed to within 15%. This calibration was then transferred to the standard CsTe diode over the wavelength range of 1450-2500Å. The calibration at wavelengths beyond 2500Å was made using interference filters. The output of the diode was compared directly with the output of the thermopile when viewing the radiation from a high intensity source transmitted by the interference filters. In late 1970 the standard detector was calibrated from 1450-2300Å by the group under Dr. Madden at the National Bureau of Standards in terms of a standard of total irradiance. A similar calibration was made by Optronic Laboratories beyond 2500Å. The agreement between the calibration at 2537Å made in early 1966 to that made in late 1970 by independent

means was better than 5%. The 1970 calibrations were used to correct the calibration of the standard detector made in 1966 and all calibrations referred to in this work reflect the 1970 measurements. A standard diode and photomultiplier combination was calibrated for the 1050-1600Å region by the sodium salicylate technique which had been referenced to the quantum efficiency of the standard diode in the 1450-1600Å region. Additional information on the long term stability with time and a high energy particle environment of the type of photodiodes used in the MUSE experiment is contained in the work of Heath and McElaney (1968).

OBSERVATIONS

Absolute Solar Irradiances

There are three types of solar uv variations which have been observed. These are the long term or solar cycle variation, those which are related to the solar rotation period, and those associated with flare activity. These are listed in order of decreasing magnitude.

The observed long term variations associated with the 11 year solar cycle (minimum late 1964, maximum late 1968) have been derived from the three uv sensors which were common to the 1966 rocket flight and the Nimbus 3 and 4 launches in 1969 and 1970 respectively. The sensor sensitivities for the three experiments are similar to those shown in figure 1 for Nimbus 3.

The sensors used in the MUSE experiments are capable of very high photometric accuracy since the noise levels are in the 10^{-14} amp range while the signal during solar observations are in the 10^{-9} to 10^{-10} amp range. Furthermore since they operate in voltage saturation range (25v) one needn't be concerned about the stability of the voltage supply.

A fundamental limitation on the determination of absolute solar irradiances is dependent upon an assumed intensity distribution with wavelength. The calculated signals for the three experiments and for the three sensors are obtained using the experimentally determined sensitivity curves and the following compilations of solar radiation:

(1) 1027-1775Å (Hinteregger et al., 1964)

(2) 1800-2600Å (Detwiler et al., 1961)

(3) 2600-4000Å (Tousey, 1963)

The ratios of the calculated signals to those observed are given in table 1 under column (a). It is readily apparent that sensor B with its peak efficiency at 1700A indicates that the solar irradiance in this wavelength region is considerably less than that used in calculating the sensor response. The solar irradiances observed with sensor B correspond to an equivalent black body temperatures of 4485 K in Aug. 1966, 4715 K in April 69, and 4635 K in April in the vicinity of 1750A. The accuracy to which these fluxes have been measured is probably better than ±15% or about ±40 K.

Satellite observations of H Lyman alpha during the operational period of Nimbus 3 have been reported by Timothy and Timothy (1970) in which they quote a value of 3.6×10^{11} quanta/cm^2 sec or 5.9 erg/cm^2 sec.

Recent satellite observations covering a 27 day period beginning July 13, 1968 of the solar irradiance have been reported by Prag and Morse (1970). Their sensor 1600-2100A, measured a flux which would be produced by an equivalent black body temperature of 4440 ± 80°K. This is about 150°K outside the experimental limits of the MUSE, sensor B and their 1600-2100A sensor.

Recently, new observations of the solar intensity in the far ultraviolet have been reported. Rocket-borne spectrophotometer observations of the solar spectrum between 1400 and 1875, which were made on September 24, 1968, and have been reported by Parkinson and Reeves (1969). Also photographic measurements of the solar uv continuum which were made from a rocket flight on July 27, 1966 have been reported by Widing et al., (1970).

Column (b) in Table 1 is calculated using the H Ly α flux of Timothy and Timothy (1970), the other emission lines from Hinteregger et. al., (1964) and a solar continuum of 4500°K based on the work of Parkinson and Reeves (1968). The ratios in column c were calculated using an equivalent black body temperature of 4500°K(66), 4700°K(69), and 4650°K(70).

The MUSE sensor response distributions functions are given in figure 2. The response distribution function at λ represents the part of the sensor output which comes from solar wavelengths less than λ. The flux values used in computing the response curves are those stated in table 1, where column-b was used in calculating the A curves except for 3' where the column-a values were used. The sensor-B curves were computed using column-c. All of the sensor-C curves

were derived from column-a fluxes. The numbers 3 and 4 refer to the appropriate Nimbus spacecraft, and R refers to the rocket flight.

The measurements of the solar irradiance which were made with the double monochrometer (10A bandpass) of the Nimbus 4, Backscatter Ultraviolet experiment are given in table 2. A comparison of the Nimbus 4 observations with a revision at the NRL data by Thekaekara (1970), that of Labs and Neckel (1968), 1970) Makarova and Kharitonov (1969), and Tousey (1963) is shown in figure 3. Note however that the values of solar irradiance are integrated over 100A intervals except for Nimbus 4 and the values from Labs and Neckel (1968) beyond 3275A. The best overall agreement from 2550-3400A appears to be with the compilation by Makarova and Kharitonov (1969). Below 3000A there is good agreement with the NRL rocket data (Tousey, 1963), however at longer wavelengths the solar irradiances are considerably lower than the NRL data. The MUSE observations on Nimbus 4, sensor c, show an indication although not outside the experimental error that in the region of overlap where 50% of the response is from solar radiation in the 2790-3090A region the solar radiation is slightly greater than that indicated in the NRL data.

The most significant solar cycle variation is observed in the radiation which originates near the region of solar temperature minimum. In August 1968 the solar irradiance observed by sensor B at 1750A was only 41% of that observed in April 1969. In April 1970 the irradiance had decreased to 76% of its value one year earlier. Additional support for believing these changes to be real can

be seen in sensor C, peak response about 2900A where the same trend is observed but not of the same magnitude as sensor B. On the other hand column-b under sensor A indicated that H Ly-α has not changed significantly during this period. These variations are of the order of the 27 day variation which have been observed.

The solar cycle variation of the solar flux in the vicinity of 1750A should produce significant changes in the production rate of atomic oxygen in the lower thermosphere-upper mesosphere region. A discussion of the importance of dissociation in the tail of the Schumann-Runge continuum and predissociation of the vibrational levels above $v' = 2$ ($\lambda < 1972$A) of the $B^3 \Sigma_n^-$ of this system has been given in detail by Hudson, et al. (1969).

An increase in the producetion rate of atomic oxygen in the mesosphere-lower thermosphere region without a corresponding change in the photodissociate rate of O_3 would lead to an increase in the amount of ozone. There is some experimental evidence that this may be taking place. Gattinger and Jones (1966) observed a fourfold decrease in the twilight brightness of the 0, 1 band of the O_3, $^1\Delta_g - {}^3\Sigma_g$ system between 1960 and 1964. One of the theories for the production of $O_2(^1\Delta_g)$ is via the photodissociation of O_3 in the Hartley continuum. Additional experimental evidence has been given by Paetzold (1961) who reported a small enhancement in the amount of ozone above 35 km which was greater in 1958 than in 1952, and which showed a small positive correlation with sunspot numbers and the dm solar radio flux.

27 Day UV Variability

The most clearly observed uv flux variability is that associated with the 27 day solar rotational period. These variations are easily observed since the amount of sensor degradation in that period is small. After 12 months of operation the sensor currents had decreased to 9.3% for sensor (A), and 70% for sensors (B) and (C) of their initial values. During the succeeding six months the output decreased an additional 39%, 29%, and 11% respectively.

The decrease of the signal with time can be approximated quite well with an exponential decay. A graph of the log of the sensor current with time can be fitted by a series of straight lines whose slope decreases with the passage of time. The sensor currents with the exponential decay removed are given in figure 4 for one year. Each data point represents a daily average of readings at the terminator (1-8 per day).

At present the data from Nimbus 3 and 4 are being examined in detail for a yearly variation in the uv flux. After corrections are made for the change in distance from the sun, and very slight changes in the angle of solar illumination of the sensors due to the non uniform orbital motion of the earth it appears that there is a significant enhancement which was a maximum in December of 1969 and 1970. This effect is not shown in figure 4 where only simple exponential decoy factors were taken out to show the 27 day variations.

Shown for comparison purposes are several indicators of solar activity. The 8-20A X-ray flux background (flare enhancements removed) is from the experiment on Explorer 37 of R. Kreplin of the Naval Research Laboratory. The values for the daily ΣK_p and the 10.7 cm solar flux are taken from "Solar-Geophysical Data" of the Environmental Data Service NOAA. Active solar regions producing enhancements in the 8-20A X-ray flux and the 10.7 cm radio flux are definitely related to the uv enhancements. In addition it appears that some relationship does exist between the solar wind related perturbations of the geomagnetic field through K_p. When $\Sigma K_p > 40$ it frequently is observed to follow 0-3 days after a uv maximum which sometimes does not correlate well with the other solar activity indicators.

The uv maxima and minima correlate better with the 10.7 cm radiation than with the calcium plage area or the Zurich provisional mean sunspot numbers. At best the correlation between the uv and 10.7 cm radiation is poor as can be seen in figure 5 for sensor (A). Similarly Timothy and Timothy (1970) have observed that the correlation between the EUV helium II Lyman α line at 304A with the standard indicators of solar activity is poor. For the MUSE experiment the correlation is much worse for the longer wavelength sensors (B) and (C).

A graph of the log of the percentage variation of irradiance versus the wave number (cm^{-1}) of the point where the response curve is 0.5 produces an approximate straight line as shown in figure 6. This could be used as an empirical guide to estimate the variation which one might expect to see in the region

spanned by sensors A and C. No scientific justification is proposed for this relation.

It can be seen in figure 4 that frequently one observes two uv maxima per solar rotation for sensors A and B. A graph of the Carrington longitude of the central meridian on the days of the uv maxima is given in figure 7 which covers a period of 28 solar rotations. The uv maxima can be determined with an accuracy of about ±1 day or ±13° in longitude. Two distinct phenomena are observed. First the uv maxima appear to originate from two uv active region, as seen be the clustering of the points about two straight lines. The regions have persisted through 28 solar rotations, and they have been observed by the MUSE experiments on Nimbus 3 and 4. The longitude of the strongest or primary feature is indicated by (x) whereas the secondary region is described by (o). At the time of launch of Nimbus 3 the two regions were separated in longitude by 225°, and 28 rotations later. The separation had decreased to 190°. If one uses 13.199°/day as the rotation rate of the Carrington longitude, then the rotation rate of the primary uv active region is 13.14°/day while that of the secondary one is 13.11°/day.

The time dependence of the variations of the uv irradiances (sensor A) per solar rotation are given in figure 8 for the two regions shown in figure 7. The primary region peaked during solar rotation 1548 while the secondary one appears to have reached a maximum around rotation number 1557.

Evidence for the existence of persistent zones of activity on opposite sides of the sun has been presented by Dodson (1970) and Bumba (1970). In general the active regions appear to be better defined in the uv. Also there is an approximate agreement as to strength and longitude of the active regions as determined from ground based and satellite uv measurements.

Flare UV Variability

On April 21, 1969 at 19:59 U. T. a major optical flare of optical importance 3B, small class X was recorded. The response of the experiment to this flare is shown in figure 9. The ordinate is the sensor current normalized to the value at the terminator on orbit 101. The function $f(\theta)/\cos\theta$ represents the sensor response function to changing angles of illumination of the photocathode. The flare occurred during orbit 102, 15 frames or 12 minutes prior to sun appearing in the field of view. Only the shortest wavelength channel showed any flare enhancement. If an exponential decay for the flare radiation is assumed, then this leads to an enhancement of 16% above the pre and post flare values of solar radiation which produces the signals in the shortest wavelength channels. Based on the sensor response functions given in figure 2, the enhancement shown for sensor A should be due principally to H, Ly-α.

REFERENCES

Bumba, V., Large-scale magnetic field and activity patterns on the sun, Leningrad Symposium, IUCSTP, May 1970 (in press).

Detwiler, C. R., Garrett, D. L. Porcell, J. D., and Tousey, R., The intensity distribution in the ultraviolet solar spectrum, Ann. Geophys., 17, 263, 1961.

Dodson, H. W., Comments on large scale organization of solar activity in time and space, AIAA Bulletin, 7, 563, 1970 (Abstract).

Gattinger, R. L. and Jones, A. V., The $^1\Delta_g - {}^3\Sigma_g^+$ O_2 bands in the twilight and day airglow, Planet. Space Sci., 14, 1, 1966.

Heath, D. F. and Sacher, P. A., Effects of a simulated high-energy space environment on the ultraviolet transmittance of optical materials between 1050 and 3000A, Appl. Opt., 5, 937, 1966.

Heath, D. F. and McElaney, J. H., Effects of a high-energy particle environment on the quantum efficiency of spectrally selective photocathodes for the middle and vacuum ultraviolet, Appl. Opt., 7, 2049, 1968.

Hinteregger, H. E., Hall, L. A., and Schmidtke, G., Solar XUV radiation and neutral particle distribution in July 1963 thermosphere, Space Research V, Amsterdam, North Holland Publ. Co., 1175, 1964.

Labs, D. and Neckel, H., The radiation of the solar photosphere from 2000A to 100 , Z. Astrophys., 69, 1, 1968.

Labs, D. and Neckel, H., Transformation of the absolute solar radiation data into the 'International Practical Temperature Scale of 1968,' Solar Phys., 15, 79, 1970.

Makarova, E. A. and Kharitonov, A. V., Mean absolute energy distribution in the solar spectrum from 1800A to 4mm, and the solar constant, Soviet Astronomy A. J., 12, 599, 1969.

Paetzold, H. K., The photochemistry of the atmospheric ozone layer, Symposium on Chemical Reactions in the Lower and Upper Atmosphere, Stanford, 1961.

Parkinson, W. H. and Reeves, E. M., Measurements in the solar spectrum between 1400 and 1875A with a rocket-borne spectrometer, Solar Phys. 10, 342, 1969.

Prag, A. B. and Morse, F. A., Variations in the solar ultraviolet flux from July 13 to August 9, 1968, J. Geophys. Res., 75, 4613 (1970).

Thekaekara, M. P., Proposed standard values of the solar constant and the solar spectrum, J. Environmental Sc., 13, 1970.

Timothy, A. F. and Timothy, J. G., Long-term intensity variations in the solar helium II Lyman alpha line, J. Geophys Res., 6950, 1970.

Tousey, R., The extreme ultraviolet spectrum of the sun, Space Sci. Rev., 2, 1, 1963.

Widing, K. G., Purcell, J. D. and Sandlin, G. D., The uv continuum 1450-2100A and the problem of the solar temperature minimum, Solar Phys., 12, 52, 1970.

Table 1

Ratio of Calculated to Observed Signals

Vehicle (yr)	A			B			C	
	a	b	*	a	c	*	a	*
Aerobee (1966	1.26	1.13	0.47	4.83	1.04	0.54	1.26	0.54
Nimbus 3 (1969)	1.69	1.15	0.47	1.98	0.93	0.47	0.83	0.59
Nimbus 4 (1970)	0.94	0.83	0.47	2.60	1.06	0.61	0.87	0.30

[a] Signals calculated using the tabulated fluxes by Hinteregger et al., (1964), Detwiler et al., (1961), and Tousey (1963).

[b] Signals calculated using H Ly α flux of Timothy and Timothy (1970), other emission lines from Hinteregger et al., (1964), and a solar continium at 4500 °K.

[c] Signals calculated using equivalent blackbody temperatures of 4500 °K (66), 4700 °K (69), and 4650 °K(70).

* Effective operture of sensor (cm^2).

Table 2

Solar Irradiance Measured with a 10A Bandpass and Triangular Slit Function

Vacuum Wavelength (A)	Irradiance (ergs/cm^2-sec-A)
2557.0	10.7
2736.8	23.5
2830.7	39.1
2876.7	39.0
2922.6	63.8
2976.2	61.9
3020.3	49.0
3059.0	63.2
3125.9	71.0
3176.2	82.3
3312.9	94.6
3399.4	96.4

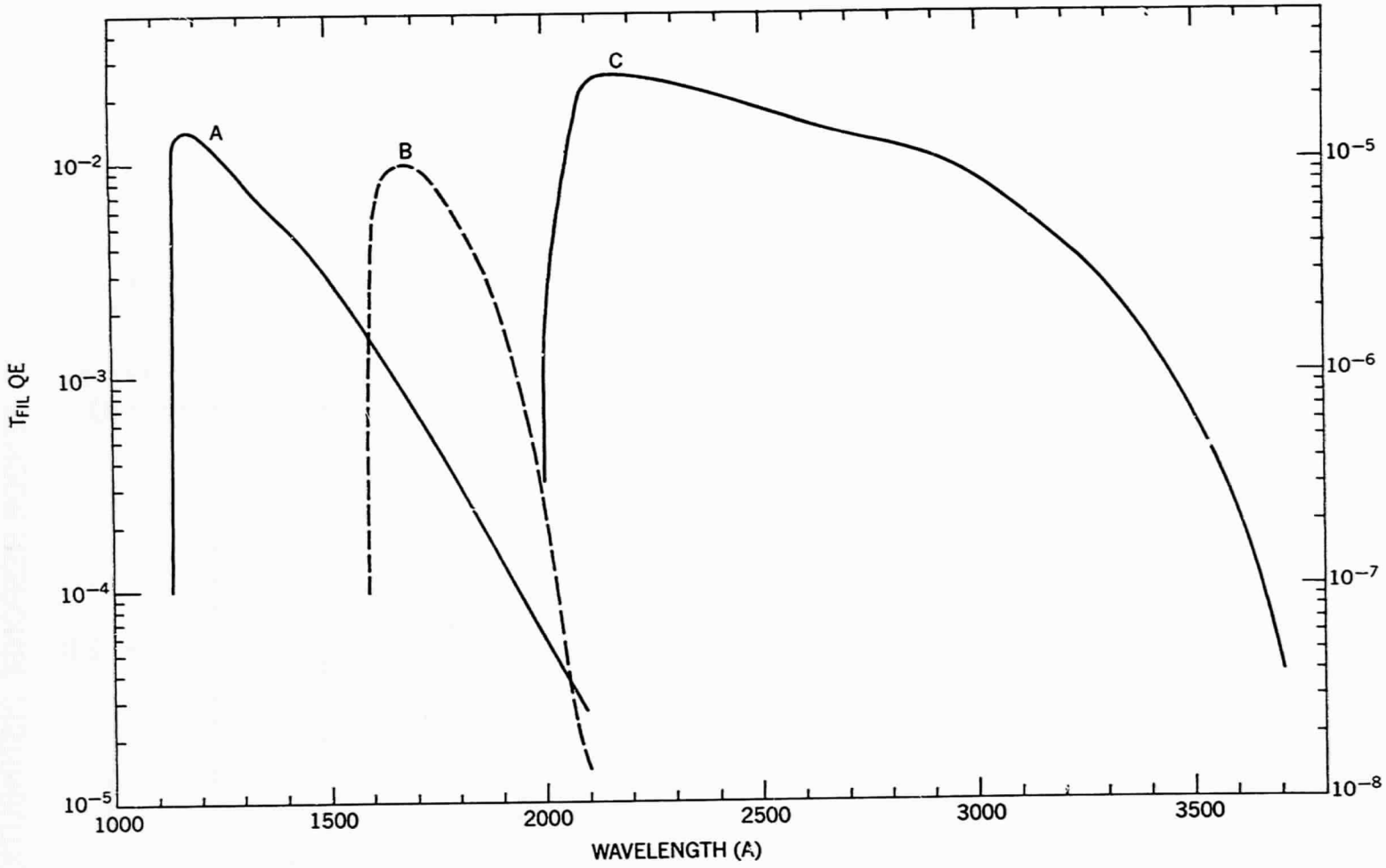

Figure 1. Product of filter transmittance and photocathode quantum efficiency. The left ordinate refers to A and B while the right ordinate is for C.

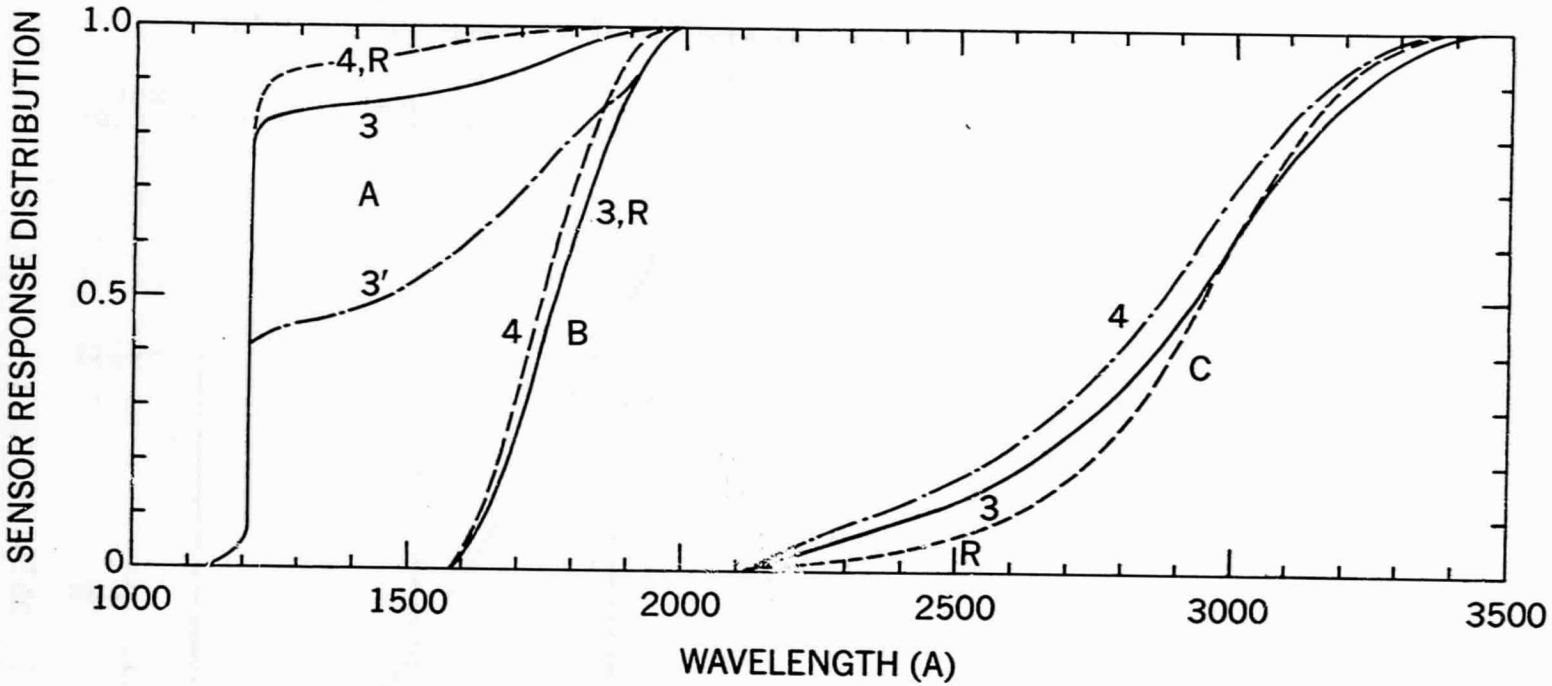

Figure 2. Sensor response distribution is the fractional part of the total signal coming from wavelengths, less than λ. The A, B, C, designates the sensors which are referred to in table 1 and Figure 1. The curves R, 3 and 4 refer to the rocket, Nimbus 4 instruments respectively; and were calculated using fluxes specified in column-b (sensor A), column-c (sensor B,) and column a (sensor C). The 3' curve was calulated from the column-c fluxes.

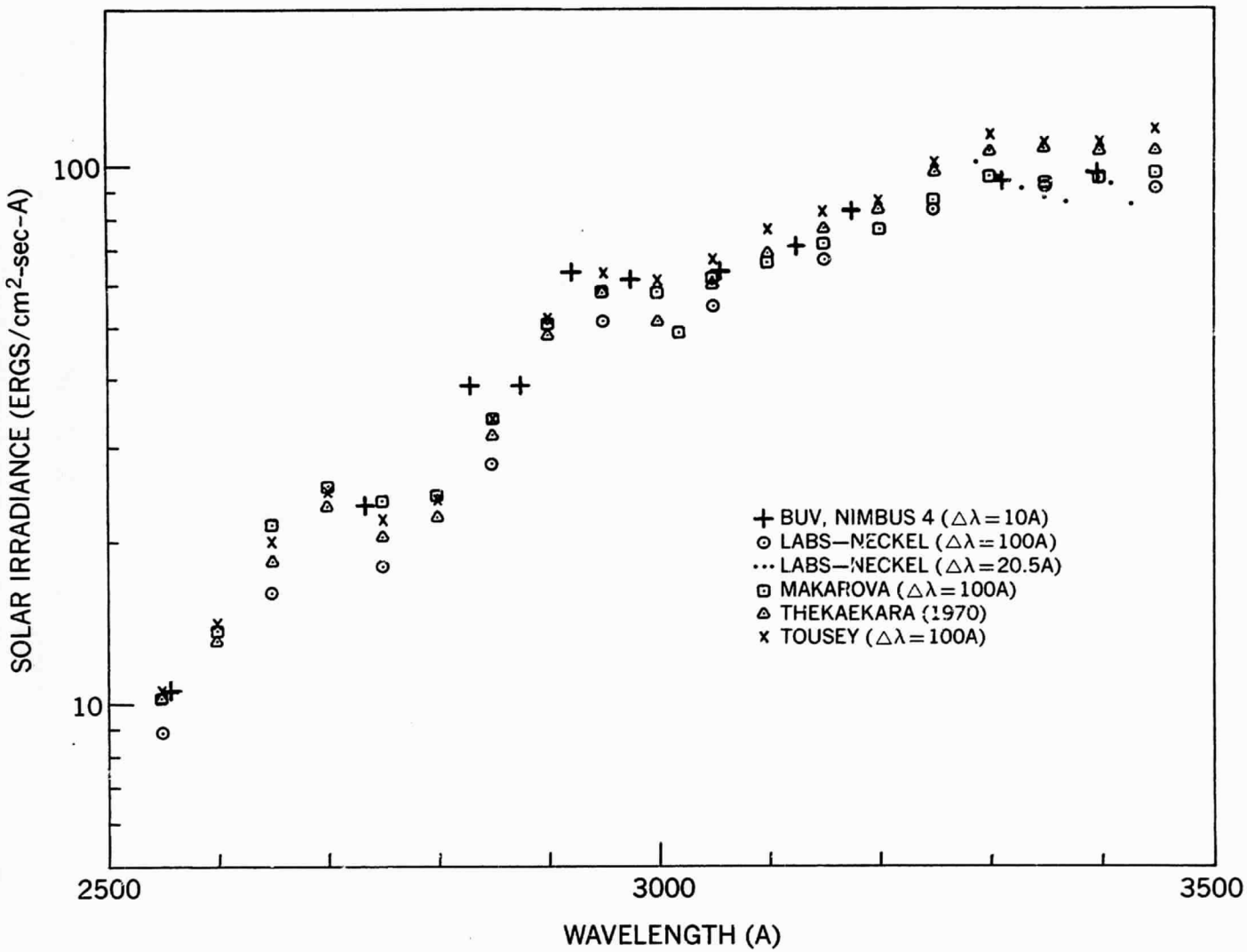

Figure 3. Comparison if solar irradiance from Nimbus 4 with the Thekaekara (1970) Labs and Neckel (1968, 1970), Makarova and Kharitonov (1969) and Tousey (1963).

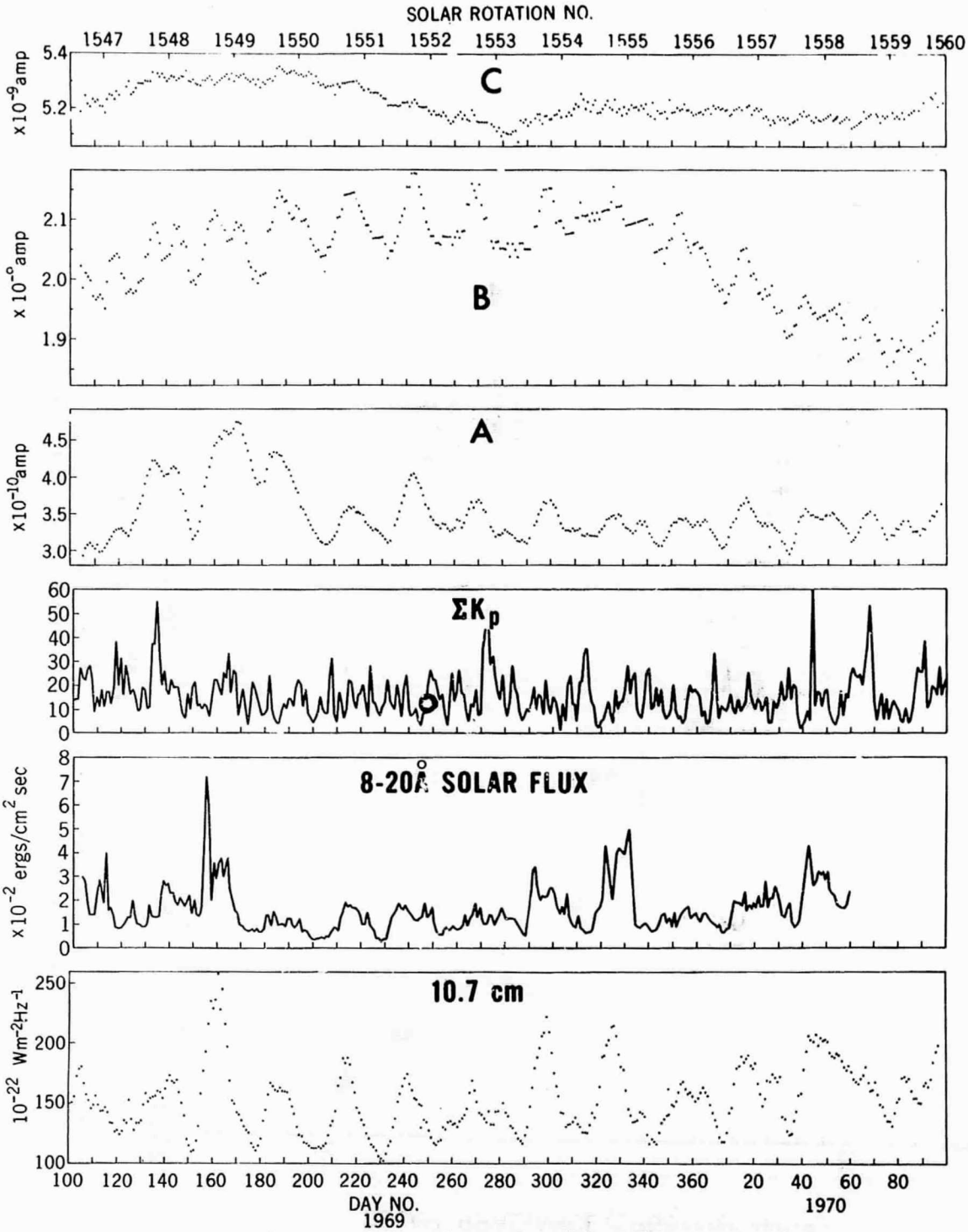

Figure 4. Sensor currents with exponential decay factors removed compared with other indicators of solar activity.

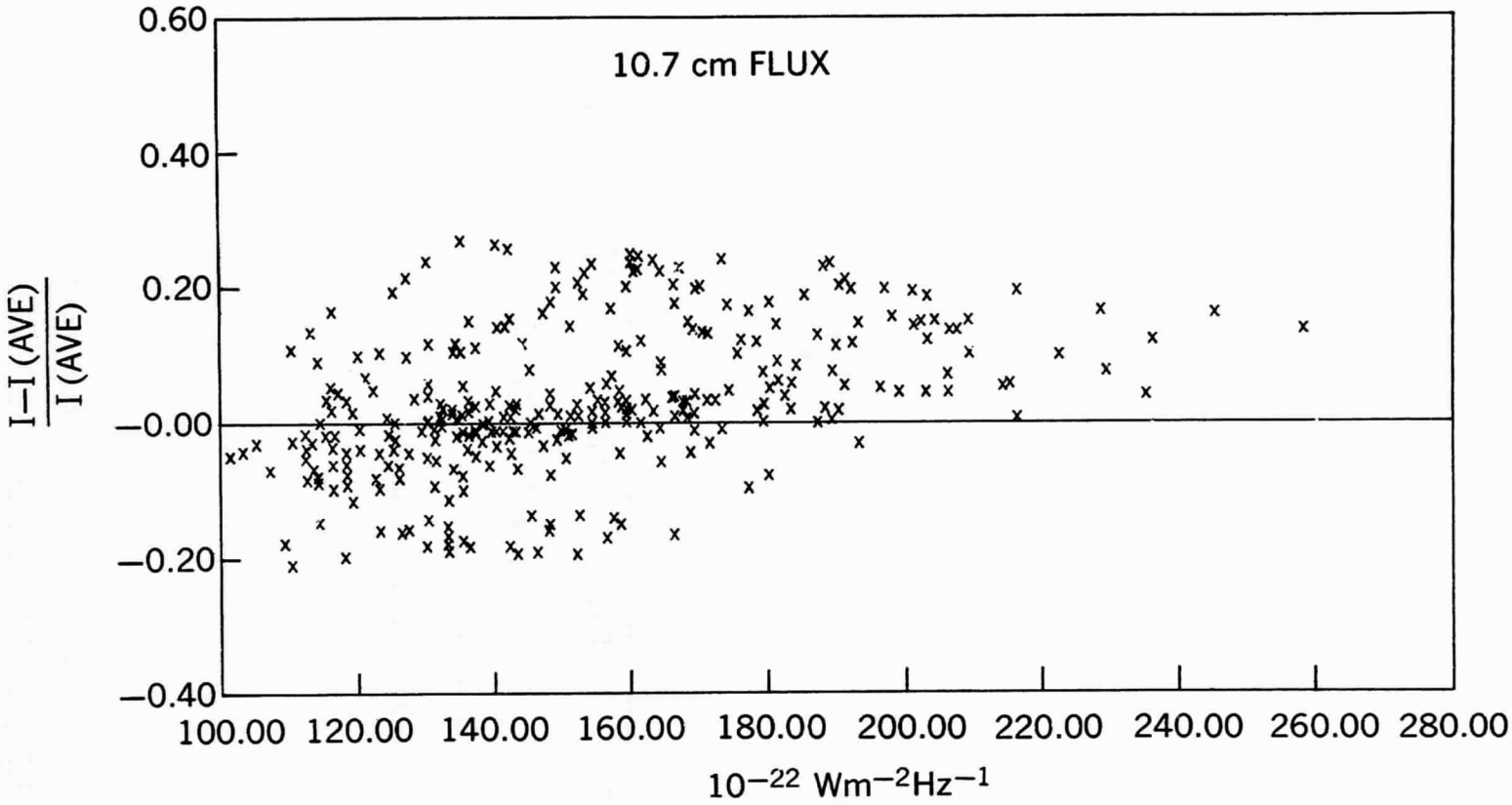

Figure 5. Relation between solar irradiances changes in the uv (sensor A) and at 10.7 cm.

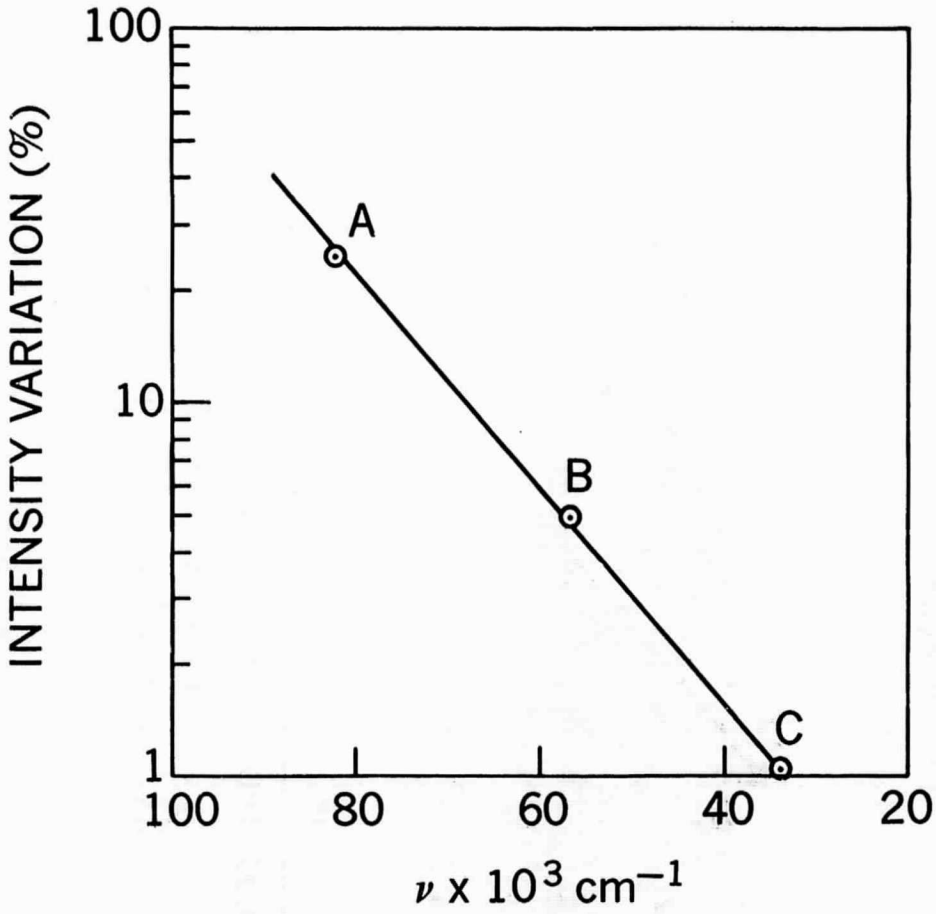

Figure 6. Percentage uv variation typically observed with the three sensors versus the wavenumber of the 0.5 point of the response distribution given in figure 2.

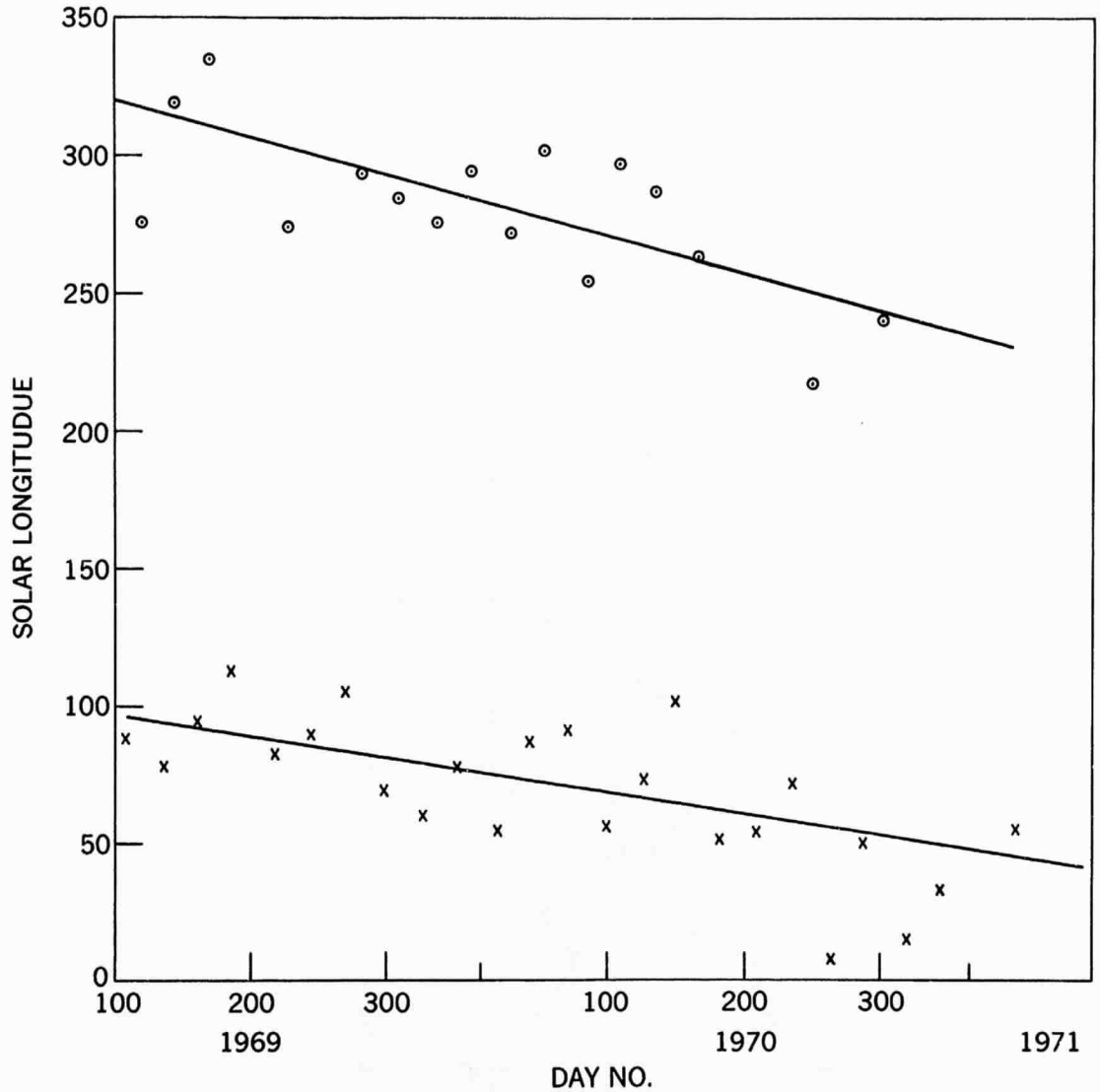

Figure 7. Carrington longitude of the central meridian at the time of observed uv maxima. The stronger region is indicated by (x) while the secondary region is shown by (⊙).

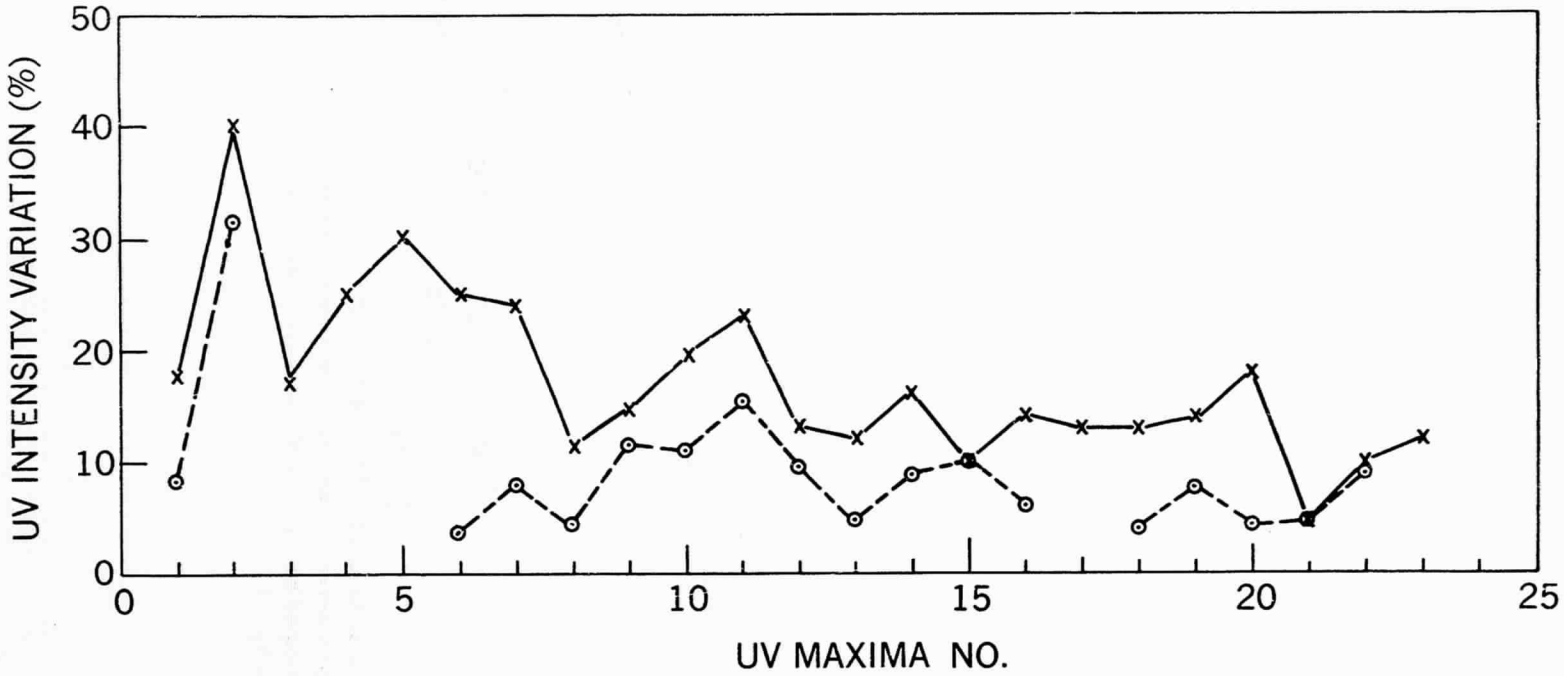

Figure 8. Time dependence of the uv intensity variation observed for the two active regions.

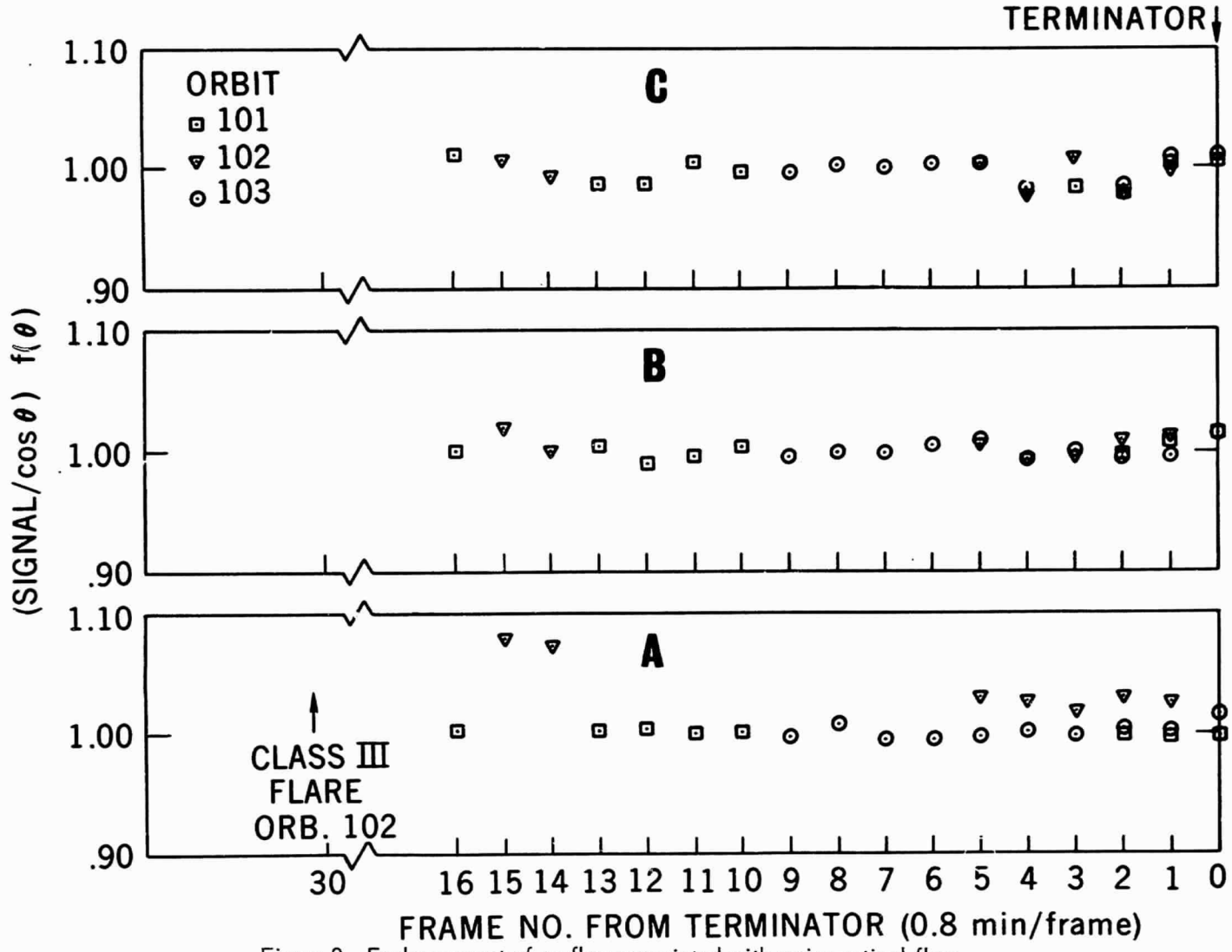

Figure 9. Enchancement of uv flux associated with major optical flare.